Probing Protein Structure by Solvent Perturbation of NMR Spectra: The Surface Accessibility of Bovine Pancreatic Trypsin Inhibitor

Henriette Molinari,* Gennaro Esposito,# Laura Ragona,§ Monica Pegna,¶ Neri Niccolai,‖ Roger M. Brunne,** Arthur M. Lesk,## and Lucia Zetta§

*Istituto Policattedra, Università di Verona, 37100 Verona, Italy; #Dipartimento di Scienze e Tecnologie Biomediche, Università di Udine, 33100 Udine, Italy; §Laboratorio NMR, CNR, 20131 Milan, Italy; ¶ITALFARMACO, Cinisello Balsamo, 20100 Milan, Italy; ‖Dipartimento di Biologia Molecolare, 53100 Siena, Italy; **Bayer AG, Wuppertal 1, D-42096, Germany; and ##University of Cambridge, MRC, Cambridge CB2 2QH, England

ABSTRACT In the absence of specific interactions, the relative attenuation of protein NMR signals due to added stable free radicals such as TEMPOL should reflect the solvent accessibility of the molecular surface. The quantitative correlation between observed attenuation and surface accessibility was investigated with a model system, i.e., the small protein bovine pancreatic trypsin inhibitor. A detailed discussion is presented on the reliability and limits of the approach, and guidelines are provided for data acquisition, treatment, and interpretation. The NMR-derived accessibilities are compared with those obtained from x-ray diffraction and molecular dynamics data. Although the time-averaged accessibilities from molecular dynamics are ideally suited to fit the NMR data, better agreement was observed between the paramagnetic attenuations of the fingerprint cross-peaks of homonuclear proton spectra and the total NH and H^{α} accessibilities calculated from x-ray coordinates, than from time-averaged molecular dynamics simulations. In addition, the solvent perturbation response appears to be a promising approach for detecting the thermal conformational evolution of secondary structure elements in proteins.

INTRODUCTION

Spin labels covalently bound to biomolecules (receptors, enzymes) or to ligands (spin-labeled substrate or inhibitor analogs) may act as reference centers for distance determination in NMR studies and therefore have been widely employed to obtain information on the geometry of the binding sites (Wien et al., 1972; Dwek et al., 1975; Campbell et al., 1975; Schmidt and Kuntz, 1984; Moonen at al., 1984; Kosen et al., 1986; Anglister et al., 1984a,b; Arean et al., 1988; Williams, 1989).

The binding of spin-labeled oligonucleotides to single-stranded DNA-binding proteins as monitored by 2D NMR difference spectroscopy has also been reported (De Jong et al., 1988). The covalently spin-labeled nucleotide broadens the resonances of the protein hydrogen spin systems around the binding site because the magnetic dipole of its unpaired electron increases the relaxation rate of the nuclei. Because the resonance linewidth is an inverse function of the transverse relaxation time, the affected resonances are consequently broadened or disappear. Hence the NMR difference spectra (presence versus absence of the bound spin label) lead to the identification of the resonances originating from the residues located in the region of the combining site. This dipolar editing of the NMR spectrum of a protein may be considered the result of a selective paramagnetic perturbation because large dipolar effects die off quite quickly with the distance, although they are detectable up to 15–20 Å (Schmidt and Kuntz, 1984).

Perturbation of NMR relaxation in proteins by soluble spin labels has been suggested by us and by others (Esposito et al., 1989, 1992, 1993a,b; Petros et al., 1990, 1992; Fesik et al., 1991; Niccolai et al., 1991; Improta et al., 1994a,b; Scarselli et al., 1995) as a tool for obtaining information about groups on the surface of the macromolecule.

As a further contribution to this approach, we describe here studies of the NMR spectrum of bovine pancreatic trypsin inhibitor (BPTI) as a function of added water-soluble spin label. BPTI is a small protein whose structure has been characterized by excellent NMR, crystallographic, and molecular dynamics studies (Berndt et al., 1992, and references therein). This model system has been used to assess the correctness of the methodology and the reliability of the approach for further structural studies on unknown proteins, stable folding intermediates, and interaction processes. The comparison of the presented NMR-derived surface accessibilities with those obtained from x-ray diffraction and molecular dynamics data offers new perspectives for the use of soluble paramagnetic probes, together with useful guidelines for data treatment and analysis.

MATERIALS AND METHODS

TEMPOL (4-hydroxy-2,2,6,6-tetramethyl-piperidine-1-oxyl) (Sigma) and BPTI (Fluka) were used without further manipulations.

All samples used for NMR experiments contained 2 mM BPTI in H_2O:D_2O 95:5 at pH 3.5 (uncorrected pH-meter reading). The homonuclear experiments were collected at pH 3.5 and 298 or 309 K, unless otherwise indicated; heteronuclear experiments were collected at the same pH and at 309 K.

Received for publication 11 July 1996 and in final form 19 March 1997.

Address reprint requests to Dr. Henriette Molinari, c/o Laboratorio NMR, CNR, via Ampere 56, 20131 Milan, Italy. Tel.: 02-706-43-554; Fax: 02-266-30-30; E-mail: henry@labnmr.icmnmr.mi.cnr.it.

0006-3495/97/07/382/15 $2.00

The TEMPOL:BPTI ratio (R) was chosen by reference to resonance attenuation for a CPMG spin-echo sequence after 40–50 ms transverse relaxation, resulting from adding nitroxide to a concentration of up to R = 10. All of the subsequent 2D NMR experiments were performed using R = 6 or 10.

The spectra were acquired at 500 MHz on a Bruker AM-500 spectrometer. Aliquots of a few microliters of a concentrated aqueous solution of TEMPOL (2 M) were added directly to the NMR tube. For the total correlation spectroscopy (TOCSY) and the clean TOCSY experiments (Braunschweiler and Ernst, 1983; Bax and Davis, 1985; Griesinger et al., 1988), a sweep width of 6 kHz was used in both dimensions, the acquisition time was 0.141 s in t_2, and 64 transients were collected for each t_1 increment. The total number of increments was 400. In the TOCSY experiments the MLEV-17 spin-lock sequence, preceded and followed by a 0.5-ms trim pulse, was applied for a total mixing time of 18 ms, at a r.f. level corresponding to $\gamma B_2/2\pi$ = 10 kHz. The suppression of the water signal was achieved by weak irradiation or with a DANTE (Morris and Freeman, 1978) scheme applied during the relaxation delay (2 s). The experimental data were processed on a X32-Bruker workstation, using standard UXNMR software, and weighted in either t_2 and t_1 dimensions with cosine bell functions or with 60° shifted squared sine bell functions and zero filled to 2K points in t_1 before Fourier transformation.

After Fourier transformation a polynomial routine for baseline correction was applied. Manual optimization of the instrument settings was done only once at the start of each experiment series before recording the 2D spectra in the absence of the spin label, and the settings were left unchanged after addition of the nitroxide, followed by recording of the perturbed spectra. The decrease in peak amplitude caused by added TEMPOL was evaluated from TOCSY experiments performed and processed with the same parameters.

Cross-peak volumes in the absence (V_d) and in the presence (V_p) of TEMPOL were measured by UXNMR and AURELIA softwares, with an estimated error of 10%.

For a ready classification, data are reported as individual percentage attenuation:

$$\text{Percentage attenuation} = \left[\left(1 - \frac{v_p^i}{v_d^i}\right) \times 100\right] \qquad (1)$$

where the running index i refers to the cross-peak numbering and $v_{p,d}^i$ are the autoscaled volumes of the cross-peaks, defined as

$$v_{p,d}^i = \frac{V_{p,d}^i}{(1/n)\sum_{i=1}^{n} V_{p,d}^i} \qquad (2)$$

where n is the total number of measured cross-peaks. From Eq. 2 it is readily seen that the scaling factor is simply the mean value over the n molecular locations for which a corresponding cross-peak volume can be estimated.

Most frequently we have reported a presentation of the NMR-derived attenuation figures that corresponds to the distribution of the deviation of the individual autoscaled volume ratios around their mean value, which is unitary by definition:

$$\sum_{i=1}^{n} v_{p,d}^i = 1$$

The function that was actually employed, A_N, is defined, for each observed connectivity, as

$$A_N^i = \left(2 - \frac{v_p^i}{v_d^i}\right) \qquad (3)$$

which can be easily shown to derive from recasting of

$$A_N^i = \left\{1 - \frac{V_p^i/V_d^i - \langle V_p\rangle/\langle V_d\rangle}{\langle V_p\rangle/\langle V_d\rangle}\right\}$$

where

$$\langle V_{p,d}\rangle = \frac{1}{n}\sum_{i=1}^{n} V_{p,d}^i$$

When plotted against the corresponding residue number of the molecule, the function A_N displays an attenuation dispersion map with points lying above or below the average (unitary) attenuation level.

Accessible surface areas (ASAs) were calculated from the x-ray coordinates of BPTI, obtained from the Protein Data Bank (5PTI), using a program implemented by A. M. Lesk. By analogy with the above definitions, data were discussed by means of a function (A_X) of the individual deviation of the autoscaled accessible surface areas from the mean value, according to the definition

$$A_x^i = \left\{\frac{\text{ASA}^i - \sum_{i=1}^{n}\text{ASA}^i/n}{\sum_{i=1}^{n}\text{ASA}^i/n} + 1\right\} \qquad (4)$$

Thus the values of A_X were compared directly to those of A_N.

The same procedure was followed to obtain the time-averaged accessible surface (TASA) from the structures sampled throughout the molecular dynamics trajectory (R. Brunne, 1993) and the results, expressed as A_T,

$$A_T^i = \left\{\frac{\text{TASA}^i - (\sum_{i=1}^{n}\text{TASA}^i/n)}{\sum_{i=1}^{n}\text{TASA}^i/n} + 1\right\} \qquad (5)$$

were compared to the A_N values.

The molecular dynamics simulation also provided a list of the average solvation numbers $\langle n_s\rangle$ at the various molecular positions, which we considered to represent the dynamically averaged surface area (DASA) locally sampled by the solvent. Furthermore, these data of water accessibility, expressed through the function A_D,

$$A_D^i = \left\{\frac{\text{DASA}^i - (\sum_{i=1}^{n}\text{DASA}^i/n)}{\sum_{i=1}^{n}\text{DASA}^i/n} + 1\right\} \qquad (6)$$

were compared to the A_N values.

The reported plots were produced with PC-MATLAB software.

^{1}H-^{13}C SQC correlation experiments were performed with 14 mM BPTI solutions in D_2O with sweep widths of 7.2 kHz and 20.8 kHz in F_2 and F_1, respectively. Decoupling of the heteronucleus was achieved by means of a GARP1 scheme during the acquisition, using a soft ^{13}C pulse of 50 μs. Five hundred twelve transients were collected for each t_1 increment, and a total of 384 experiments were acquired. The spectra were processed using a cosine-bell window function.

Unless otherwise stated, all of the reported comparisons refer to data obtained at 309 K. An internal standard for chemical shift measurements was not used, to avoid having to correct for differential effects of the free radical upon the solute and the reference compounds (Qiu et al., 1982). Chemical shifts were then arbitrarily referenced to the resonance of the Tyr^{21} H$^\alpha$ proton, which was set to 5.68 ppm in all of the spectra (Wagner et al., 1987).

The x-ray coordinates were displayed by using the program INSIGHT from MSI (San Diego, CA).

RESULTS AND DISCUSSION

Organic free radicals have been shown to affect both the chemical shift positions and the linewidths of NMR signals from solvents and solutes (Qiu et al., 1984). Unless independently demonstrated, the identification of a single particular mechanism responsible for a shift of the resonances is generally not possible, because several shift-inducing

processes may be operative simultaneously at the molecular level. However, the observed change in chemical shift, $\Delta\delta$ (regardless of the mechanism involved), has been interpreted as an indication of the strength of the interaction between the free radical and the proton donor or, more generally, the electron acceptor (Bonesteel et al., 1992). In the two-dimensional experiments, performed at 309 K on BPTI with a TEMPOL:protein ratio of 6:1 ($R = 6$), the maximum shift observed for a given cross-peak was 0.01 ppm, i.e., comparable to the experimental digital resolution.

The linewidths of the resonances increase because random collisions and specific interactions between solute/solvent nuclei and the free radical shorten T_2 as well as T_1 relaxation times.

When no chemical interaction occurs, the proton-electron intermolecular dipolar coupling is modulated by the translational diffusion motion, with a correlation time (τ_D) related to the corresponding coefficient, as described by Hubbard's theory (Endo, 1977). If a labile molecular complex is formed instead, the proton-electron intermolecular dipolar coupling is modulated by the molecular motion of the whole complex, by the dissociation kinetics and by the electron relaxation, and the solute/solvent relaxation may be viewed using the Solomon-Bloembergen theory (Solomon and Bloembergen, 1956). Here the relevant correlation time depends on the relative time scale of the modulating processes, of which only the dissociation exchange is related to the lability of the molecular adduct of the solute/solvent with the free radical. Only for really labile complexes (i.e., with a lifetime $\tau_m < 10^{-5}$ s) can a nonselective paramagnetic perturbation model be safely adopted.

The resonance attenuation observed upon addition of the spin label is proportional to the molar fractions of the protein and of the free radical, indicating that a model based on statistical collisions fits our data well. Indeed, when TEMPOL paramagnetic perturbation was applied to the study of gramicidin in different solvents, we observed more pronounced effects in solvents with large molar volumes, such as $CHCl_3$ (1/13.5 dm^3/mol^{-1}) and dimethyl sulfoxide (DMSO) (1/14 dm^3/mol^{-1}), than in solvents with a smaller molar volume, such as water (1/55 dm^3/mol^{-1}). In dilute equimolar solutions where the solute molar fractions increase with the solvent molar volumes, the statistical paramagnetic perturbation propagates with the inverse square ratio of the solvent molar volumes (e.g., $DMSO/H_2O = (55/14)^2$) (Niccolai et al., 1991).

A statistical interaction regime should rule out any specific interactions that could lead to conformational modifications of the protein that may affect the cross-peak amplitudes of either scalar (COSY, TOCSY) or dipolar (NOESY) 2D correlation spectra.

Earlier studies evaluated the effects of paramagnetic filtering on polypeptides, such as camel β-endorphin, that do not adopt any defined conformation in aqueous solution (Esposito et al., 1993b). Its molecular conformation in pure water is completely disordered, and only in the presence of micelles (Zetta and Kaptein, 1984; Zetta et al., 1990) or in some organic solvents (Lichtarge et al., 1987) can a helical structure be observed. The peptide, containing a large variety of amino acid types (polar, apolar, aromatic, and charged, overall 16 different residues), is a remarkable molecular test for the occurrence of possible preferential interactions of the paramagnetic probe with chemically different residues. Two-dimensional clean TOCSY experiments with the diamagnetic and paramagnetic solutions, were performed with a high molar ratio of TEMPOL:peptide ($R = 10$) (Esposito et al., 1993b). The attenuations for all of the backbone cross-peaks were nearly identical and primarily reflected the unhindered interaction expected from statistical collisions between the paramagnetic probe and the biopolymer molecules. Therefore, a general absence of preferential interactions between the paramagnetic probe and specific components of peptides can be inferred from these data.

Paramagnetic relaxation filtering effects are not identical in TOCSY and in NOESY spectra of slowly tumbling molecules, as discussed earlier (De Jong et al., 1988; Esposito et al., 1992), and we chose to perform TOCSY-type experiments in which the effects are more pronounced in view of the ratio $T_{2M}/T_{1M} < 1$.

The fingerprint regions of two clean TOCSY experiments, performed at 309 K, on a 2 mM sample of BPTI at pH 3.6, without and with TEMPOL ($R = 6$), are reported in Fig. 1. It is clear from the figure that some peaks appear unaffected by the nitroxide, whereas others are attenuated or even disappear.

Only the backbone hydrogen resonances have been analyzed, because, in this case, similar correlation times can be assumed to modulate the dipolar interactions that contribute to their relaxation process, and a direct correlation between different paramagnetic effects and nitroxide accessibility may be drawn.

The requirement that the comparison should be made within a homologous class of resonances (therefore within a presumably narrow range of correlation times) was already pointed out (Niccolai et al., 1991; Fesik et al., 1991).

Spectra were recorded at the optimal receiver gain, which varied between samples without and with TEMPOL, because of its effects on the linewidth of the water resonance. The recovered data sets always reproduced the same relative cross-peak intensities, except for an obvious scaling factor. Any artificial inconsistencies, including the inherent errors from the detection on distinct samples, were eliminated, in any case, by volume autoscaling (Eqs. 1 and 2) and by the subsequent data analysis.

Alternatively, the need to vary the receiver gain could be overcome by employing pulse-gradient techniques to suppress the water signal. Indeed, when the WATERGATE sequence (Piotto et al., 1992) was employed to achieve water suppression, the cross-peak volumes measured in the presence of the paramagnetic probe never exceeded the volumes of the cross-peaks of unperturbed spectra under the

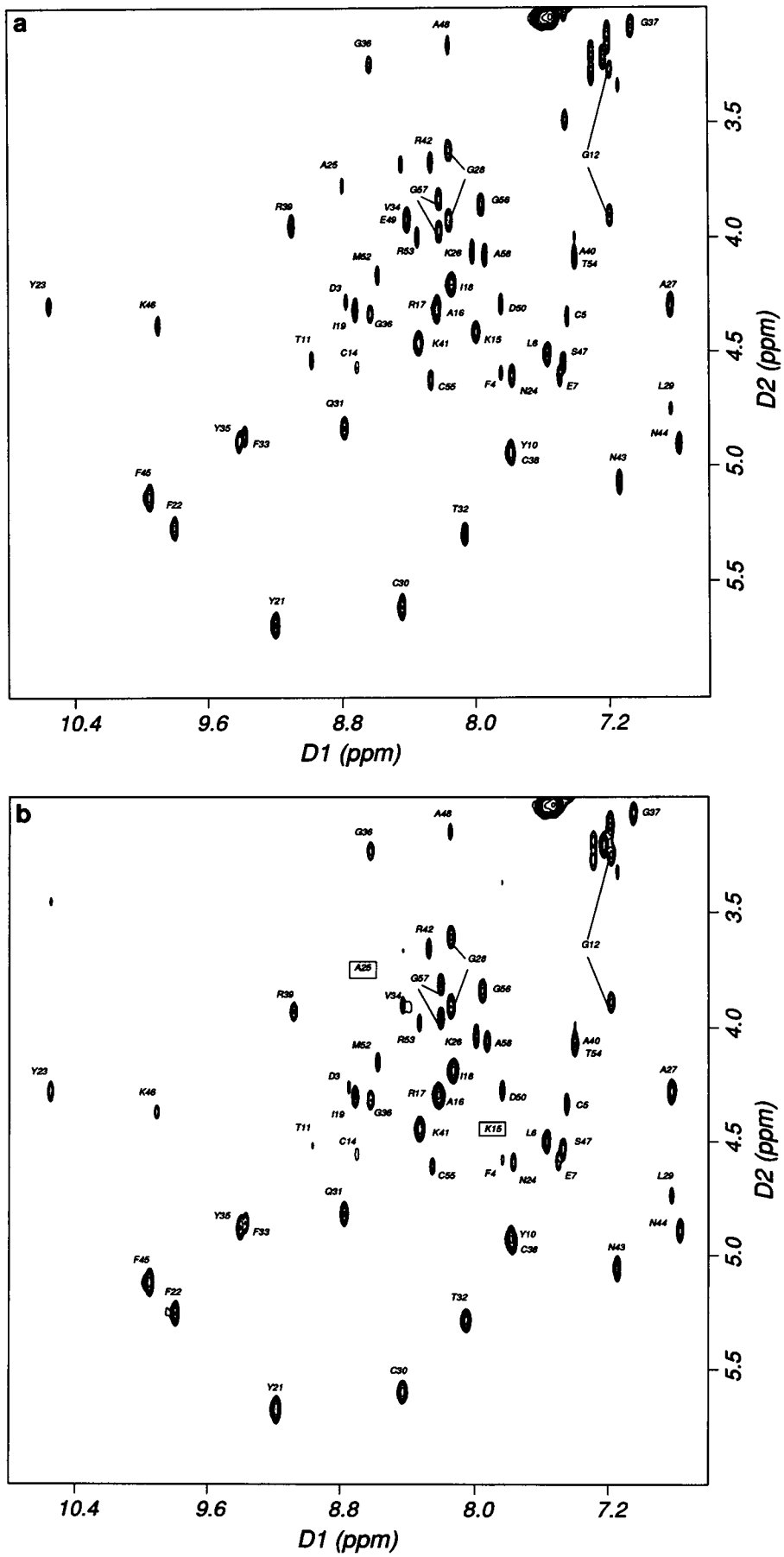

FIGURE 1 Fingerprint regions of clean TOCSY experiments of 2 mM BPTI, 309 K, pH 3.6, (*a*) without and (*b*) with TEMPOL. In the presence of TEMPOL, the cross-peaks relative to K15 and A25 disappeared. The single-letter amino acid code is used for labeling the cross-peak assignments. D1 and D2 refer to the direct and indirect acquisition dimensions, respectively. The plots were obtained with the program FELIX (MSI, San Diego, CA).

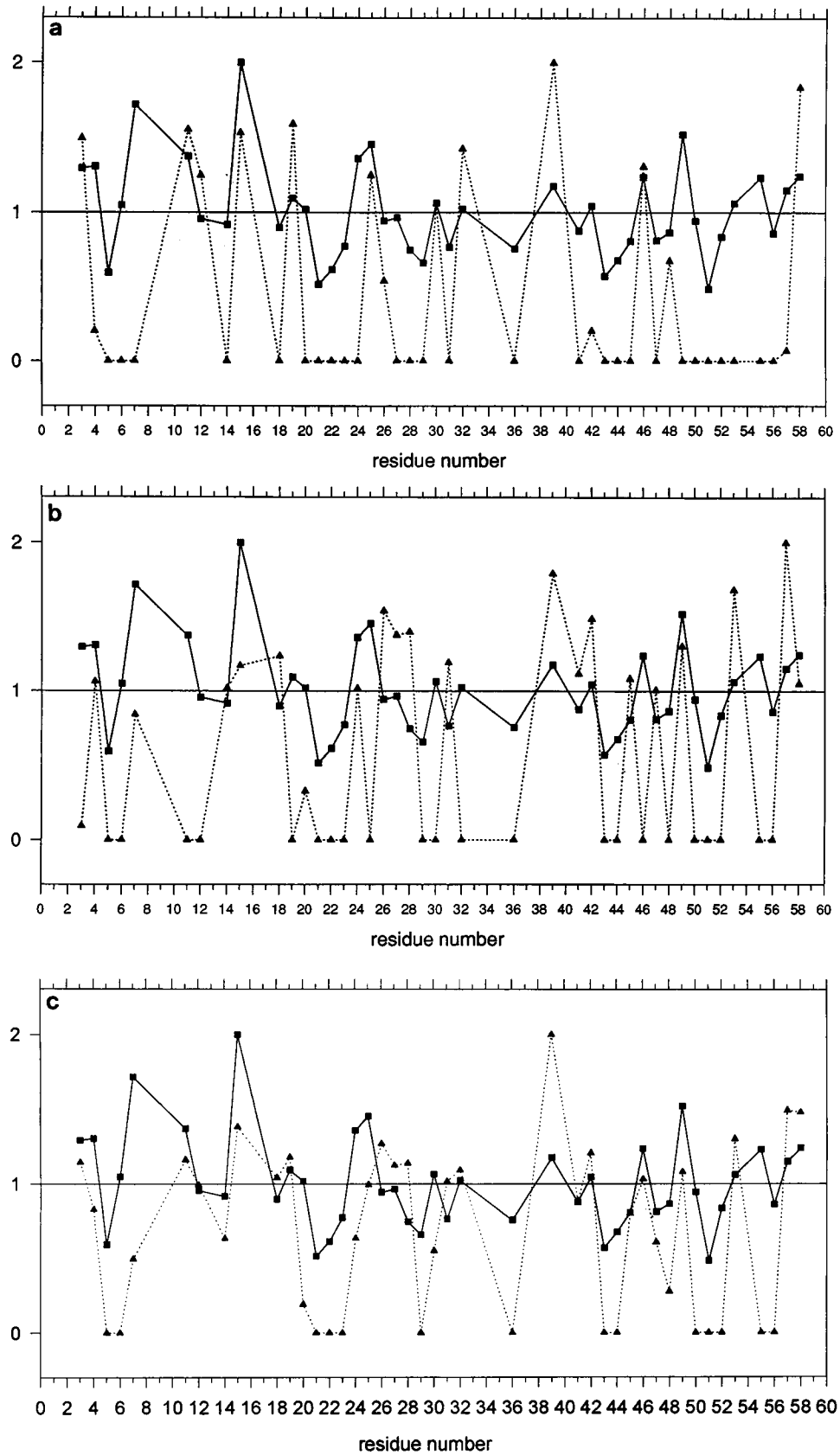

FIGURE 2 Plots of the A_N (■) and A_X (▲) values of BPTI calculated via Eqs. 3 and 4, respectively, against the residue number. The A_N values were calculated on the basis of the 43 residues for which a resolved cross-peak was observed in the ^{1}H clean TOCSY spectrum; the A_X values refer to (*a*) NH ASA; (*b*) H^α ASA; (*c*) the sum of NH and H^α ASA. For an easier comparison, rescaling over the maximum reached by A_N was applied to the A_X values larger than unity. The plotted function of A_X is defined as $f(A_X) = A_X$ for $0 \leq A_X \leq 1$, $f(A_X) = \{[(A_X - 1)/(A_X^{max} - 1)] + 1\}$ for $A_X > 1$.

same setting of the receiver gain. However, we reckon that a safer procedure, also in this case, is to analyze data by using the autoscaled volumes (Eq. 2), because acquisition conditions can never be absolutely identical with different samples.

As observed in previous similar studies, a general broadening is apparent for all of the resonances, because of the presence of the paramagnetic species in solution. In addition, more pronounced local broadenings are observed for those resonances exposed to the nitroxide.

A direct structural interpretation of absolute attenuation factors, calculated for each nucleus signal or correlation related to it, is not practical. As previously suggested (Esposito et al., 1993b), it is more convenient to analyze the paramagnetic relaxation data by discussing the relative autoscaled attenuations calculated according to Eq. 3. In this way, the function A_N versus sequence position can be plotted as reported in Fig. 2, where points lying above or below the average attenuation level are readily classified as exposed or buried molecular locations. A further advantage of this representation is the easy comparison of experiments performed under different conditions (temperature, protein and paramagnetic probe concentration, solvents). Indeed, any general effect is included in the mean value, and the observed deviations reflect only the locally induced changes.

As mentioned in Materials and Methods, a linear increase in attenuation was observed upon increasing the TEMPOL concentration. Fig. 3 shows the individual percentage attenuations (Eq. 1) of the NH-H$^{\alpha}$ connectivities of BPTI, obtained in two experiments performed with different molar ratios, i.e., $R = 6$ and $R = 10$, at different temperatures (298 and 309 K).

The relaxation effects are larger for $R = 10$ than for $R = 6$, as expected. However, the relative trend of attenuation remains mostly the same.

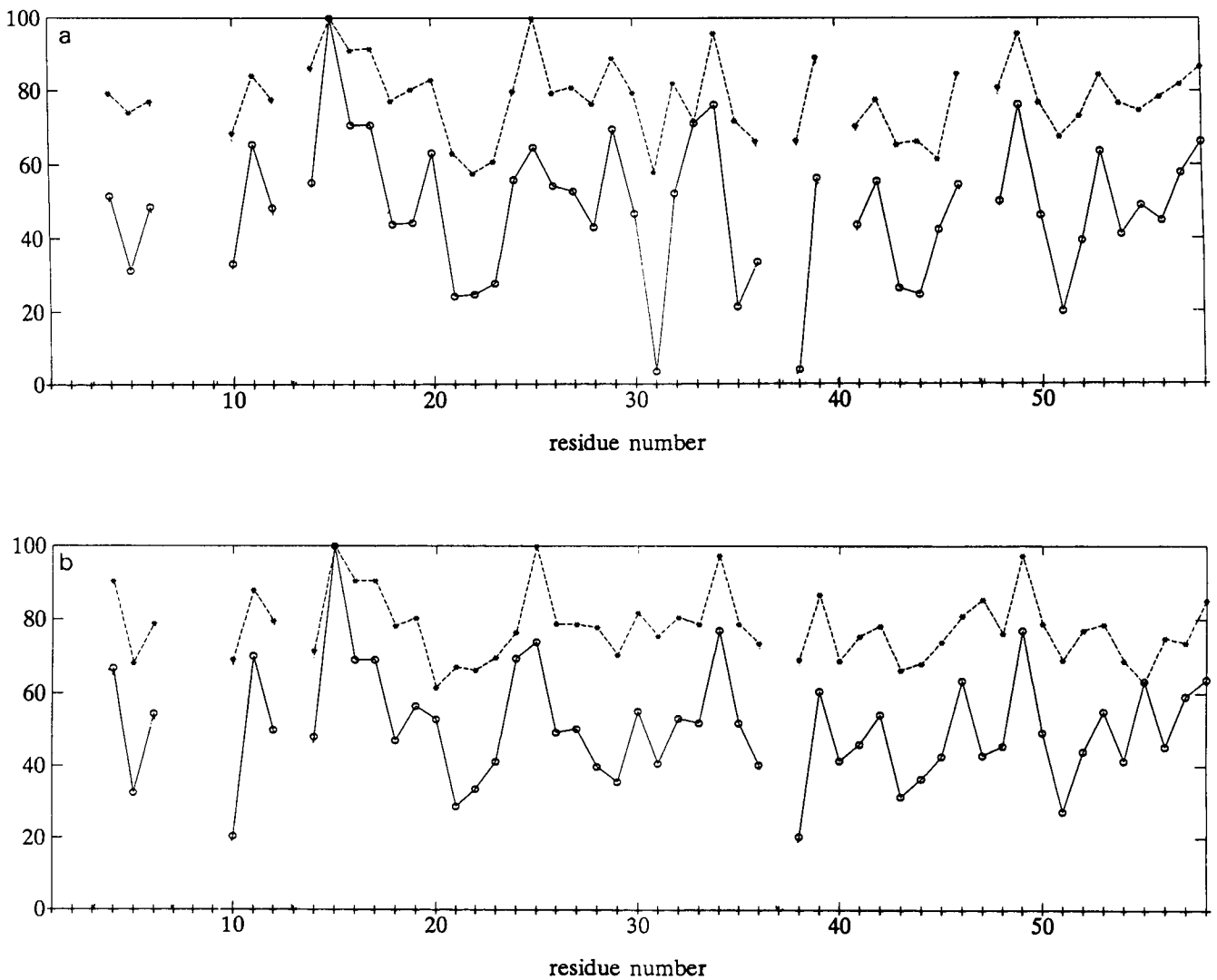

FIGURE 3 TEMPOL percentage attenuation (Eq. 1) from the NH-H$^{\alpha}$ connectivities of BPTI obtained from clean TOCSY experiments performed at (*a*) 298 K and (*b*) 309 K with different TEMPOL/BPTI molar ratios (*R*): $R = 6$ (○) and $R = 10$ (*).

TABLE 1 Surface exposure classification of the backbone hydrogens of BPTI from NMR (A_N, Eq. 3), crystal structure (A_x, Eq. 4), and molecular dynamics (A_T, Eq. 5)

Residue no.	NMR	Crystal structure			Molecular dynamics		
		NH	H_α	NH + H_α	NH	H_α	NH + H_α
1							
2							
3	e	e	ne	pe	e	e	e
4	e	ne	pe	ne	pe	e	e
5	ne	ne	ne	ne	ne	ne	ne
6	pe	ne	ne	ne	ne	ne	ne
7		ne	ne	ne	ne	pe	ne
8							
9							
10							
11	e	e	ne	pe	e	ne	pe
12	pe	e	ne	pe	e	ne	pe
13							
14	pe	ne	pe	ne	ne	e	e
15	e	e	pe	e	e	pe	e
16							
17							
18	ne	ne	e	pe	ne	pe	ne
19	pe	e	ne	pe	e	ne	pe
20	pe	ne	ne	ne	ne	ne	ne
21	ne	ne	ne	ne	ne	ne	ne
22	ne	ne	ne	ne	ne	ne	ne
23	ne	ne	ne	ne	ne	ne	ne
24	e	ne	pe	ne	ne	ne	ne
25	e	e	ne	pe	e	ne	pe
26	pe	ne	e	e	pe	e	e
27	pe	ne	e	pe	pe	e	e
28	ne	ne	e	pe	ne	e	e
29	ne	ne	ne	ne	ne	pe	ne
30	pe	pe	ne	ne	e	ne	pe
31	ne	ne	pe	pe	ne	pe	ne
32	pe	e	ne	pe	pe	ne	ne
33							
34							
35							
36	ne	ne	ne	ne	ne	ne	ne
37							
38							
39	pe	e	e	e	e	e	e
40							
41	ne	ne	pe	ne	ne	pe	ne
42	pe	ne	e	e	ne	e	pe
43	ne	ne	ne	ne	ne	ne	ne
44	ne	ne	ne	ne	ne	ne	ne
45	ne	ne	pe	ne	ne	ne	ne
46	e	e	ne	pe	ne	ne	ne
47	ne	ne	pe	ne	ne	ne	ne
48	ne	ne	ne	ne	pe	ne	ne
49	e	ne	e	pe	ne	ne	ne
50	pe	ne	ne	ne	ne	e	pe
51	ne	ne	ne	ne	ne	ne	ne
52	ne	ne	ne	ne	ne	e	pe
53	pe	ne	e	e	ne	ne	ne
54							
55	e	ne	ne	ne	ne	ne	ne
56	ne	ne	ne	ne	ne	e	e
57	pe	ne	e	e	ne	e	e
58	e	e	pe	e	e	e	e

Classification code: e = exposed (20% above the average value); pe = partially exposed (±20% from the average value); ne = not exposed (20% below the average value).

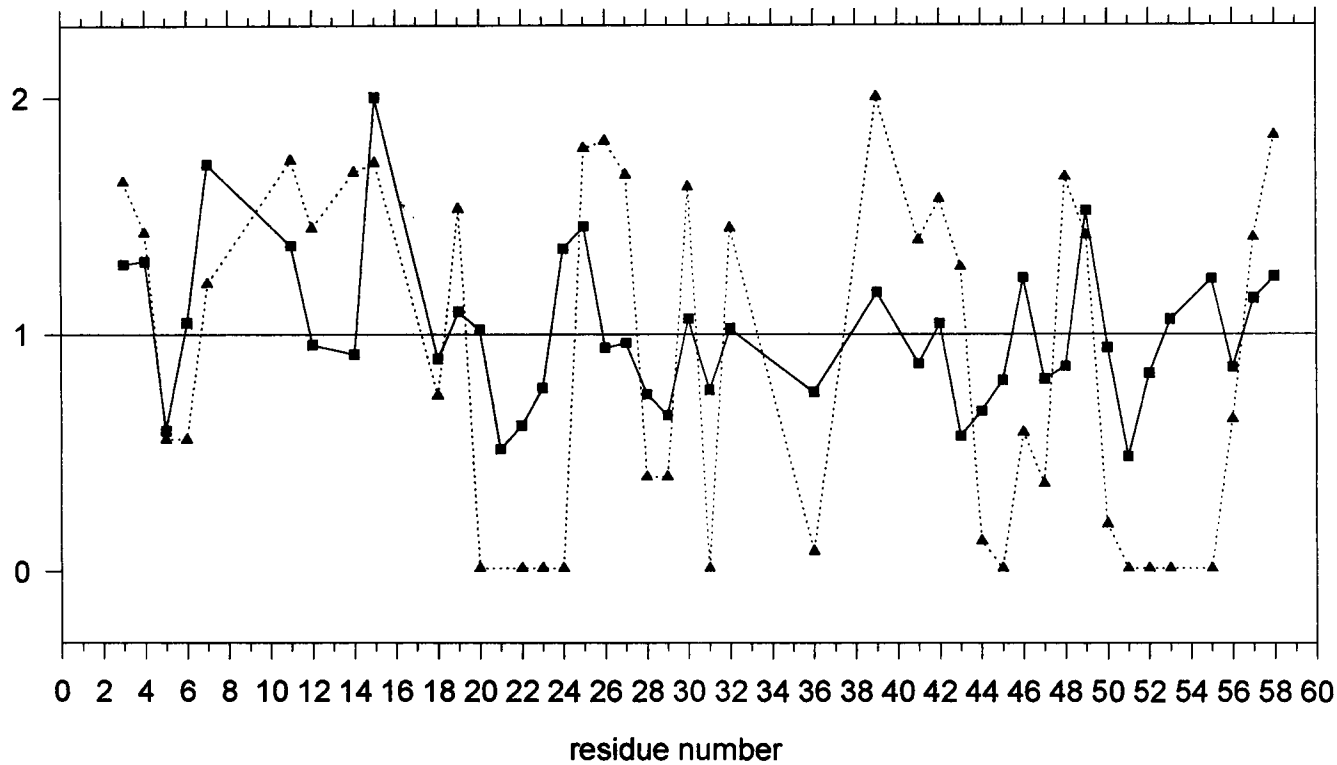

FIGURE 4 Plots of the A_N (■) and A_D (▲) values of BPTI calculated with Eqs. 3 and 6, respectively, against the residue number. The same rescaling as described in the caption of Fig. 2 was applied to the A_D values larger than unity.

In all experiment sets, the cross-peak corresponding to the NH-H$^\alpha$ correlation of K15, the center of the reactive site loop, was bleached completely upon TEMPOL addition. NMR relaxation time measurements indicate that the longest T_1 values of BPTI α-carbons are obtained for K15, N24, K46, and A58. Taking into account the V-shaped dependence of T_1 on τ_c, it has been suggested that a considerable variation in τ_c may occur at those locations (Nirmala and Wagner, 1988; Richarz et al., 1980). The experimental "singularity" of K15 was also confirmed by molecular dynamics simulations that showed a high mobility for this residue, with atomic displacements approaching 1 Å (Wlodawer et al., 1987).

Because the paramagnetic-induced relaxation is mainly due to dipole-dipole interactions between electronic and nuclear spins, the faster the motions, the less effective the electron-nuclear interactions should be in shortening relaxation times at a given frequency. Hence an increased mobility of the active site should result in a decreased attenuation of the K15 NH-H$^\alpha$ cross-peak, contrary to the experimental evidence. The TEMPOL-probed accessibility of K15 backbone hydrogens therefore arises from a high exposure of both NH and H$^\alpha$ nuclei contributing to the cross-peak, which is indeed one of the few cross-peaks where the component effects are similar. We discuss below problems that arise when opposing contributions determine the intensity of the cross-peak.

Comparison of accessibilities from NMR and x-ray data

The surface accessibilities obtained from the clean-TOCSY spectrum at 309 K ($R = 6$) and plotted according to Eq. 3 were compared with the corresponding A_X values (Eq. 4) calculated for 1) amide protons, 2) α protons, and 3) the sum of α and amide protons (see Fig. 2). All A_N and A_X values are expressed in Table 1 in terms of a ternary model (i.e., exposed, partially exposed, and not exposed).

As already pointed out, the nitroxide attenuation data from the ^{1}H TOCSY fingerprint convey information on the accessibility of the two hydrogens that contribute to the cross-peak. Some cross-peaks were not included in our analysis because partial or complete overlap at the experimental temperature prevented an accurate measurement of their volumes. It is possible to obtain complementary information when measurements are performed via heteronuclear experiments (see below).

The detailed examination of the three plots reported in Fig. 2 and the classification of Table 1 for NH (Fig. 2 *a*), H$^\alpha$ (Fig. 2 *b*), NH + H$^\alpha$ (Fig. 2 *c*) show two different kinds of local discrepancies between the individual A_X and A_N values: 1) those arising from partial differences and 2) those arising from total inconsistencies between the NMR and x-ray exposure pattern. The former discrepancies are not real conflicts because they stem from the actual nature of

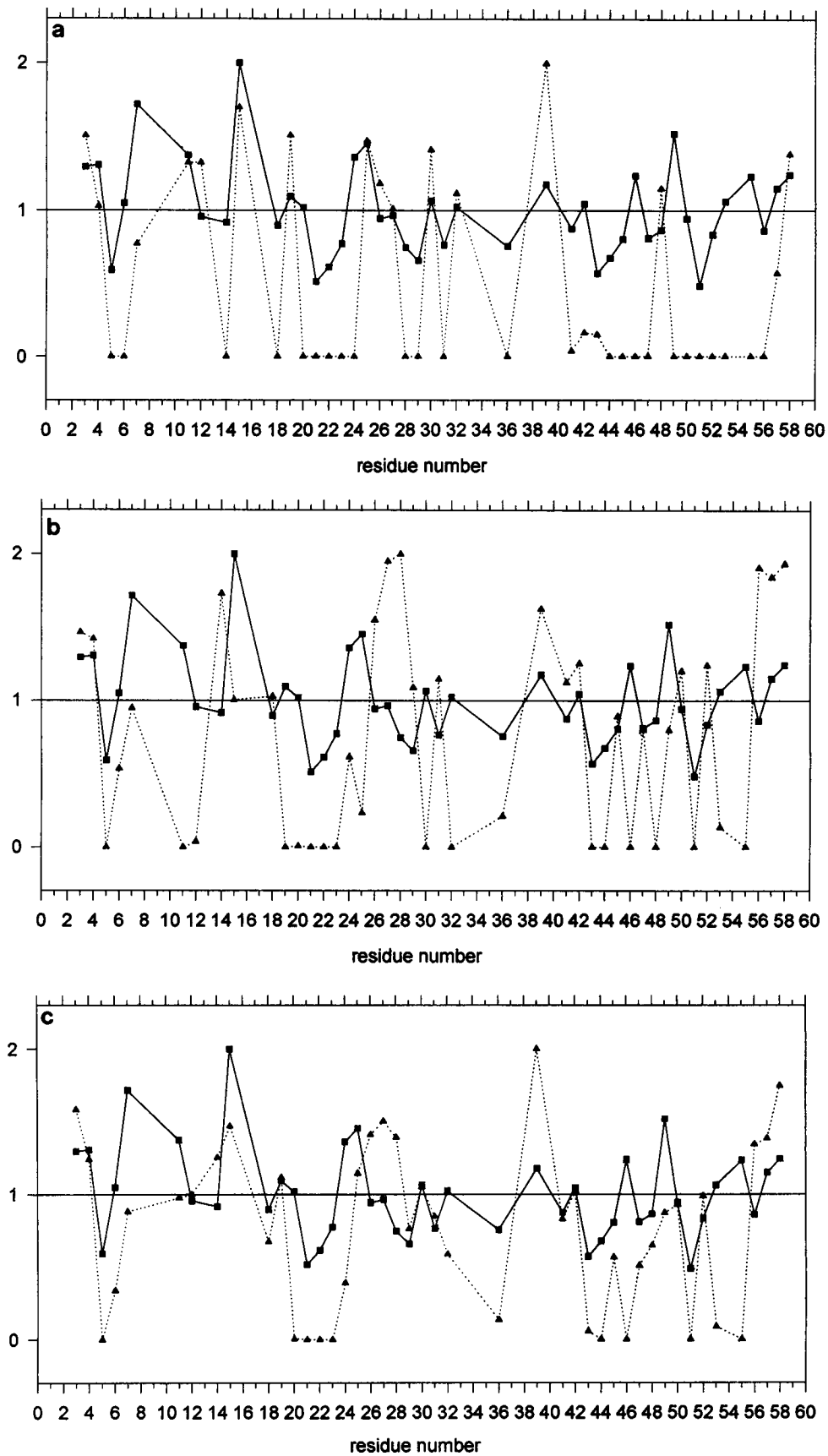

FIGURE 5 Plots of the A_N (■) and A_T (▲) values of BPTI calculated with Eqs. 3 and 5, respectively, against the residue number, for (*a*) NH; (*b*) H^{α}; (*c*) the sum of NH and H^{α}. The values of A_T larger than unity were rescaled as described in the caption of Fig. 2.

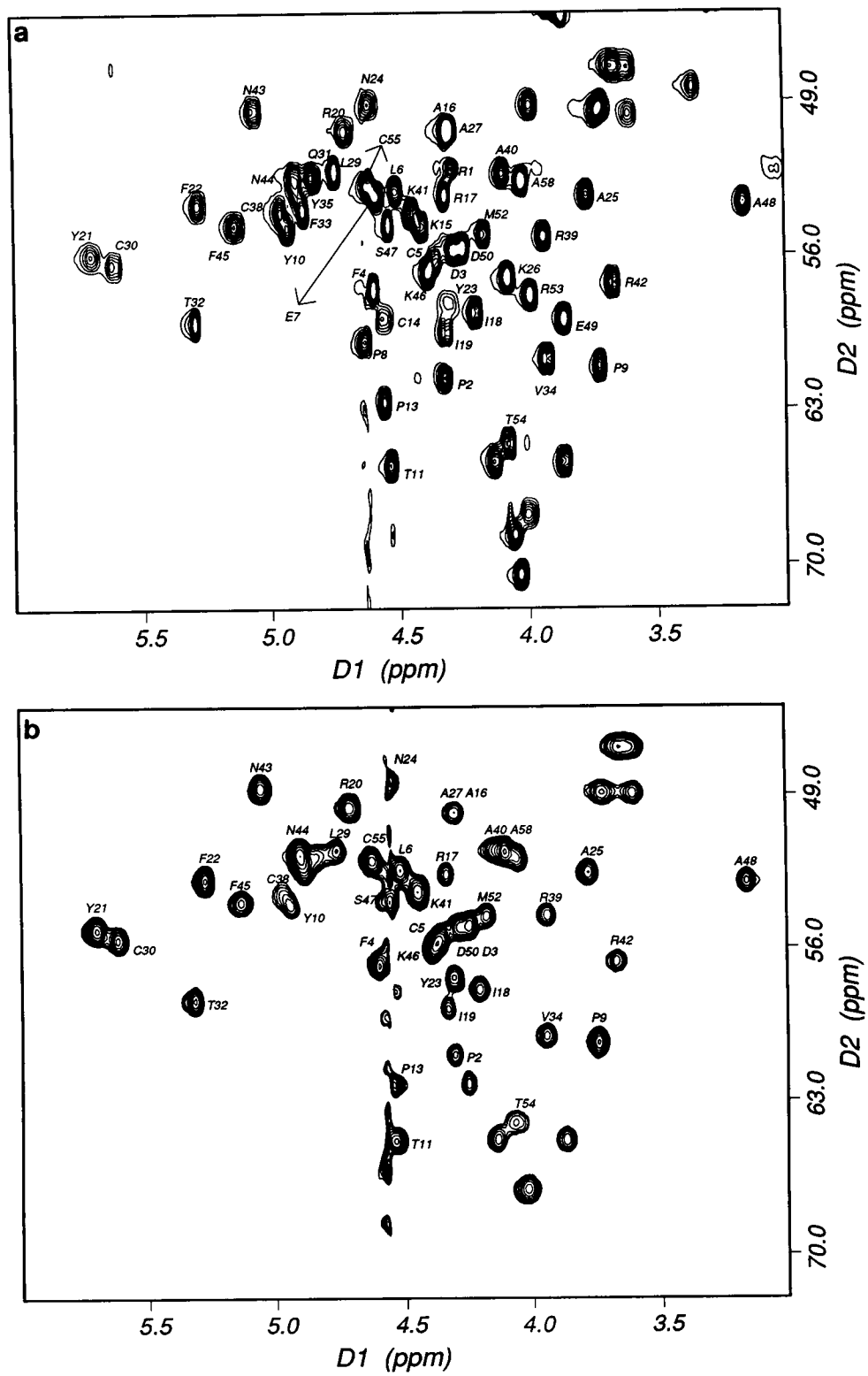

FIGURE 6 C^{α}-H^{α} region of ^{1}H-^{13}C SQC experiments performed on BPTI in deuterated water (*a*) without and (*b*) with TEMPOL ($R = 6$). The cross-peak assignments are labeled by single-letter amino acid code. D1 and D2 refer to the direct and indirect acquisition dimensions, respectively. The plots were obtained with the program FELIX (MSI, San Diego, CA).

the considered NMR observable. The NH-H^{α} cross-peak attenuations are nonlinear combinations of the individual amide and H^{α} accessibilities. As a consequence, when a single proton of the pair is exposed or buried, the observed cross-peak attenuation may either conflict or agree with the corresponding A_X value. Even the sum of the A_X values within the pair may not necessarily improve the fit because of the above-mentioned nonlinearity of the combination. The real inconsistencies between NMR and x-ray-derived exposures occur only for those residues where all of the A_X

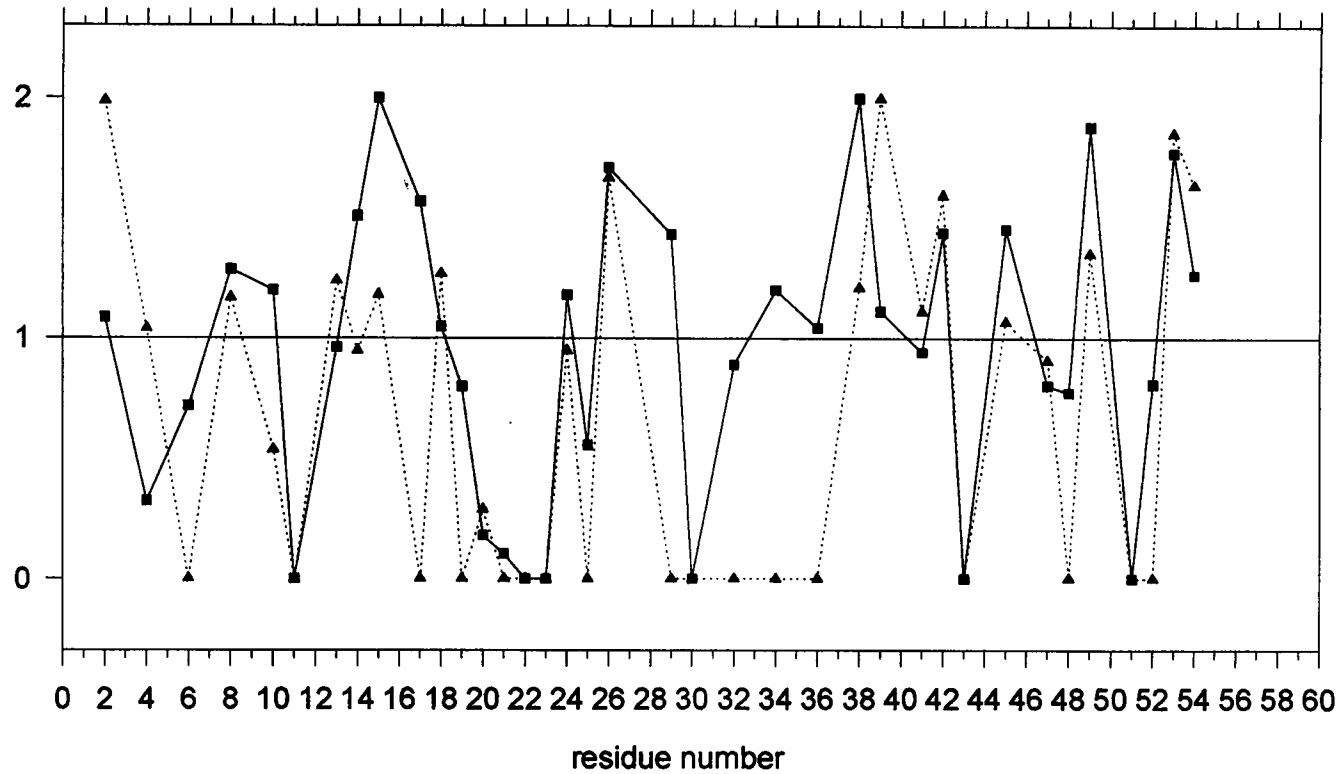

FIGURE 7 Plots of the A_N values (■) (Eq. 3) as obtained from the ^1H-^{13}C SQC spectra of BPTI and of the A_X values (▲), relative to H^α (Eq. 4) against the residue number. The reported A_N values were calculated on the basis of the 37 residues for which a resolved cross-peak was observed in the ^1H-^{13}C SQC spectrum. The A_X values larger than unity were rescaled as described in the caption of Fig. 2

values (NH, H^α, and NH + H^α) simultaneously conflict with the NMR datum. This is the case for residues 6, 7, 20, 50, and 55 (see also Table 1). For residue 20, however, the measured volumes were very weak and thus may be intrinsically affected by large errors (see below), whereas for the C-terminal segment the observed residual deviations are conceivably due to solution fraying effects.

Comparison of accessibilities from NMR and molecular dynamics

The results of a molecular dynamics (MD) study (1.4-ns trajectory) of BPTI at 277 K in the presence of water were recently reported (Brunne et al., 1993). This simulation provided a list of the average solvation number ($\langle n_s \rangle$) for the backbone amides, the total number of water molecules visiting the solvation shell within 1 ns ($\langle n_{visits} \rangle$), and a list of the atoms shielded from solvent with less than six visits per nanosecond.

We considered the individual $\langle n_s \rangle$ to report a local measure of the dynamically averaged surface area (DASA) and computed the corresponding A_D values according to Eq. 6. The A_D and A_N profiles are compared in Fig. 4.

An additional approach for comparing TEMPOL attenuation and MD data is the direct calculation of the time-averaged surface accessibility (TASA) over the structures sampled throughout the MD trajectory. TASA values were obtained as weighted averages over the mean structures calculated over four periods of the whole 1.4-ns trajectory, namely 50–100 ps, 400–800 ps, 900-1050 ps, 1100–1400 ps (Brunne et al., 1995). (The criterion for subtrajectory selection was the backbone conformational stability.)

The A_T values, calculated according to Eq. 5 for the NH, H^α, and the sum of NH and H^α, are shown in Fig. 5 together with A_N. A list of TASA ternary classification is also given in Table 1. The number of total inconsistencies (occurring at residues 6, 20, 24, 46, 49, 53, 55) is increased in this case with respect to the comparison reported between A_N and A_X values (Fig. 2). This somehow unexpected result may be ascribed to the temperature difference between dynamics (281 K) and experimental NMR data (309 K). It is well known that some thermal response differences exist among the distinct secondary structure regions of BPTI (Wagner, 1984). In particular, the worst fit is observed for the C-terminal region, where the largest effect from the temperature difference of NMR and MD data is expected, because of the hydrophobic stabilization of the α-helix fragment 48–55.

TEMPOL exposure as deduced from heteronuclear ^1H-^{13}C NMR experiments

^1H-^{13}C SQC experiments were performed on BPTI in the absence and in the presence of TEMPOL (R = 6). The

C^{α}-H^{α} regions of the two spectra are reported in Fig. 6. The overall attenuation data should substantially reflect only the exposure of the α protons, because the paramagnetic-induced effect is proportional to the magnetogyric ratio of the involved nuclei, which entails a sensitivity penalty on the effects that can be retrieved from the carbon resonance amplitudes.

The A_N function corresponding to the experimental cross-peak ratios from ^1H-^{13}C data was compared with the A_X function from the x-ray H^{α} ASA, as shown in Fig. 7.

Some of the discrepancies identified in the plots of Fig. 2 were removed, namely those from H^{α} of residues 6 and 20. However, other, previously absent deviations were found for residues 4, 10, 17, 34, and 36. (The deviation observed for residue 29 may arise from an imperfect volume estimation due to partial overlap.)

In summary, these last data show that no overall improvement of the agreement is reached upon removing the nonlinear combination of the NH and H^{α} contributions that are present in the proton data.

In view of the inherent differences between the computation of the water-accessible surface areas and the experimental assessment of exposure from TEMPOL perturbations, analysis should be mainly focused on the global trend of the functions A_N and A_X.

As a matter of fact, the best agreement among all pairs of data sets examined in the present paper was found for the comparison of A_N from proton NMR data with A_X curves, i.e., those relative to static ASAs (Fig. 2 and Table 1).

TABLE 2 Correlation between hydrogen-bond involvement and TEMPOL accessibility of the backbone amides of BPTI

	H donor	Solution*	Crystal‡	TEMPOL§
3_{10}-Helix	CYS 5 NH	7	X	ne
	LEU 6 NH	20	X	pe
β-Sheet	ILE 18 NH	20	X	pe
	ARG 20 NH	20	X	pe‖
	TYR 21 NH	19	X	ne
	TYR 23 NH	16	X	ne
	ASN 24 NH	17	X	e
β-Sheet	GLN 31 NH	20	X	ne
	PHE 33 NH	20	X	—
	TYR 35 NH	20	X	—
α-Helix	GLU 49 NH	0	X	e
	ASP 50 NH	16	X	pe
	CYS 51 NH	19	X	ne
	MET 52 NH	20	X	ne
	ARG 53 NH	20	X	pe
	THR 54 NH	20	X	—
	CYS 55 NH	18	X	e

*The listed amides are putative H-bond donors in the refined BPTI structure family obtained from NMR restraints in solution. The numbers indicate the H-bond occurrence at a specific backbone NH, within the 20 best energy conformers (Berndt et al., 1992).

‡H-bond involvement (X) of the listed backbone amides of BPTI consistent with the neutron diffraction structure of the form II crystal.

§Buffer exposure classification of the listed backbone amides of BPTI obtained from TEMPOL perturbation of NMR spectra (clean TOCSY, 309 K). See Table 1 for the exposure codes. Dashes are reported when no corresponding classification is available from the NMR data.

‖The measured volumes of the corresponding cross-peaks were affected by large errors (see text).

Correlation between TEMPOL perturbation and secondary structure

Table 2 contains a summary of TEMPOL exposures compared with the hydrogen bonding pattern reported for the secondary structure elements of BPTI (Berndt et al., 1992), i.e., 3_{10}-helix for residues 3–6, antiparallel β-sheet for segments 18–24 and 29–35, and α-helix for the segment 48–55. A good correlation was generally observed between the presence of H bonds, as reproduced by DIANA calculations, and a limited TEMPOL accessibility. Some caution is necessary when drawing this kind of comparison, because H-bond formation, although more frequent for nonsuperficial residues, is affected by local structure dynamics, which is not necessarily monitored by TEMPOL perturbation. For instance, two H-bonded amides, namely 24 and 55, appear exposed when assayed with TEMPOL. On the other hand, TEMPOL data confirm the lack of H bonds resulting from NMR restrained modeling for Glu^{49} amide proton, contrary to the crystal structure data.

Nitroxide perturbation experiments were also performed at 298 and 341 K to investigate the ability of the method to assess the stability of secondary structure elements. The behavior observed upon temperature increase should reflect a balance of the following effects: 1) a decreased efficiency of the diffusion-controlled dipolar relaxation (Aime et al., 1993), and 2) an increased frequency of collisional events.

The observed TEMPOL accessibilities at 298, 309, and 341 K are reported in Fig. 8. The trends observed at the three temperatures are in agreement with the reported conformational stability of BPTI. A closer inspection reveals that, as the temperature is raised, the TEMPOL accessibility decreases for the N- and C-terminal segments and increases for the central antiparallel β-sheet stretch (region 18–35) and the fragment 40–45.

These findings are consistent with expectations based on the local stability of secondary structure elements of BPTI, which were obtained by H-D exchange studies (Wagner et al., 1984). In particular, the hydrophobic stabilization of the helical segments is nicely reflected by the decrease in TEMPOL accessibility with the increase in the temperature. On the contrary, the reduced efficiency of the hydrophilic interactions with the increase of the temperature leads to loosening of the β-sheet and of the appended segment 40–45, as reflected by an increased TEMPOL accessibility. These results appear even more valuable, in terms of sensitivity of the approach, in consideration of the high thermal stability of BPTI. Thus the TEMPOL perturbation method may be employed to study the structural dynamics of proteins either before or during thermal denaturation, as previously anticipated (Esposito et al., 1992).

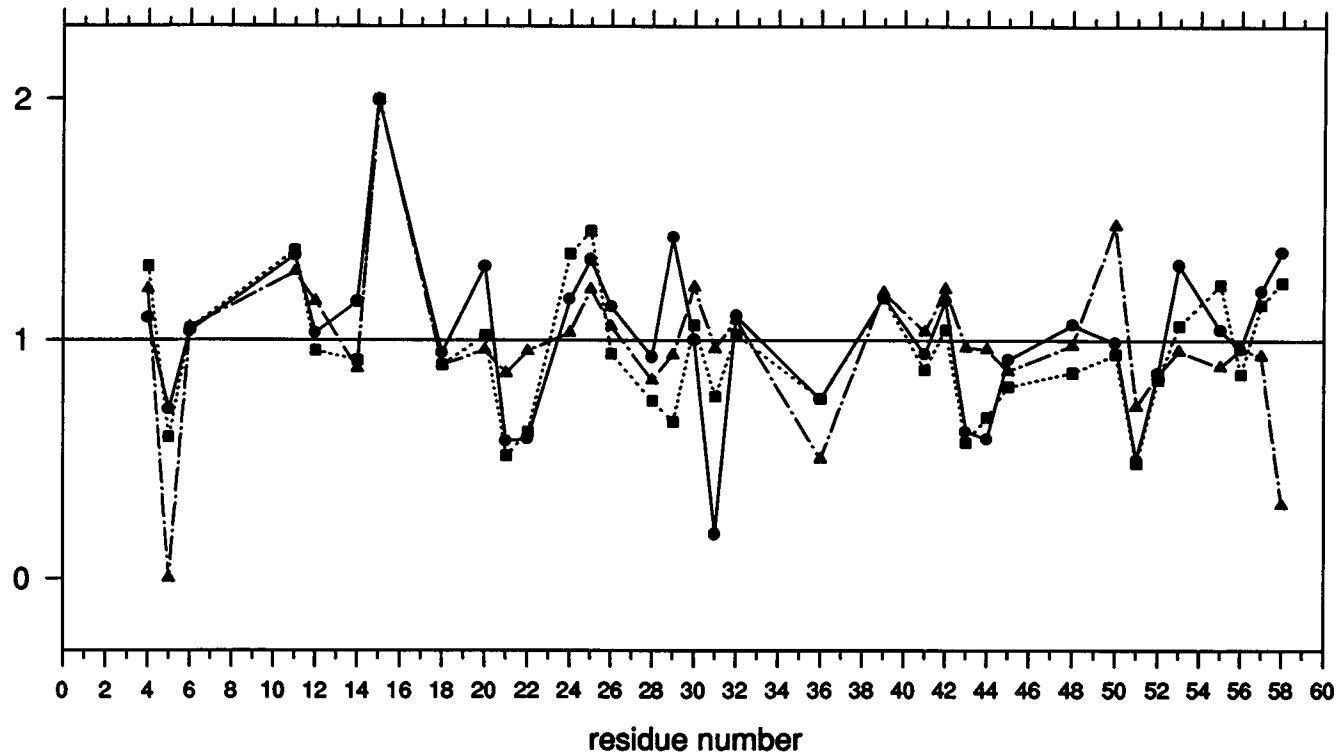

FIGURE 8 Plots of the A_N values (Eq. 3) relative to the fingerprint cross-peaks as detected from ^{1}H clean TOCSY spectra of BPTI at 298 K (●), 309 K (■), and 341 K (▲) versus residue number.

CONCLUSIONS

By using BPTI as a model compound, we have outlined the quantitative reliability of a procedure for the identification of solvent-exposed regions of biomolecules, based on the change in the relaxation rate that is caused by the addition of a paramagnetic probe.

We have shown that there are no specific interactions between TEMPOL and the studied molecule. No proton chemical shift change has been observed for BPTI upon TEMPOL addition. Similar results were previously observed with lysozyme (Esposito et al., 1992), camel β-endorphin (Esposito et al., 1993b), and bovine α-lactalbumin (Improta et al., 1995a,b).

Possible artefacts arising from the measurement of cross-peak volumes in the presence of a paramagnetic species have been carefully analyzed. An experimental protocol for the data acquisition, together with an analytical procedure for their treatment, by volume autoscaling, has been suggested.

A critical effort was put into the search for appropriate accessibility parameters, derived from static (x-ray) and dynamic (MD simulations) data, which could better represent the exposure probing parameters obtained by NMR. It has been shown that although in principle the time-averaged accessibilities from molecular dynamics simulations at the suitable temperature may better reproduce the experimental TEMPOL-exposure data, the homonuclear ^{1}H experiments afford the best agreement with the accessible surface areas calculated from x-ray coordinates and in particular with the sum of NH and H^α accessibilities. If an experiment can be performed in which the cross-peaks report the exposure of a single atom, such as the ^{1}H-^{13}C heteronuclear experiment discussed in the text, the agreement does not necessarily improve. In fact, the inherent differences between the computed water-accessible surface areas and the exposures probed by TEMPOL perturbation are even more highlighted when single atomic locations are considered.

Perhaps the most interesting finding of the present study comes from the ability of the nonselective paramagnetic perturbation approach to detect the conformational evolution of secondary structure motifs with temperature. The results obtained in the presence of TEMPOL by increasing the temperature up to 341 K satisfactorily reproduce the expected changes in the secondary structure elements of BPTI, as discussed in the text. This adds confidence in applying the method to the analysis of protein folding intermediates, where segments or specific residues of a protein may change their exposure along the pathway between the native and denatured states.

Thanks are due to Varian for supplying facilities for gradient-NMR experiments, to Prof. A. Sironi for helpful suggestions, and to F. Greco for skillful technical assistance.

HM, LR, and LZ acknowledge the financial support from "Programma finalizzato Chimica Fine e Secondaria" and the "Associazione A. De Marco." NN acknowledges the financial support from "Progetto Strategico Biologia Strutturale."

REFERENCES

Aime, S., M. Botta, E. Carreno, P. L. Anelli, and F. Uggeri. 1993. $Gd(DOTP)^{5-}$ Outer-sphere relaxation enhancement promoted by nitrogen bases. *Magn. Reson. Med.* 30:583–586.

Anglister, J., T. Frey, and H. M. McConnell. 1984a. Magnetic resonance of a monoclonal anti-spin label antibody. *Biochemistry.* 23:1138–1142.

Anglister, J., T. Frey, and H. M. McConnell. 1984b. Distance of tyrosine from a spin-label hapten in the combining site of a specific monoclonal antibody. *Biochemistry.* 23:5372–5375.

Arean, C. O., G. R. Moore, G. Williams, and R. J. P. Williams. 1988. Ion binding to cytochrome. *Eur. J. Biochem.* 173:607–615.

Bax, A., and D. G. Davis. 1985. Practical aspects of two-dimensional transverse NOE spectroscopy. *J. Magn. Res.* 65:355–360.

Berndt, K. D., P. Güntert, L. P. M. Orbons, and K. Wüthrich. 1992. Determination of high-quality nuclear magnetic resonance solution structure of the bovine pancreatic trypsin inhibitor and comparison with three crystal structures. *J. Mol. Biol.* 227:757–775.

Bonesteel, J. K., B. Borah, and R. D. Bates, Jr. 1992. Effects of nitroxide free radicals on proton donor chemical shifts. *J. Magn. Res.* 98:477–482.

Braunschweiler, L., and R. R. Ernst. 1983. Coherence transfer by isotropic mixing: application to proton correlation spectroscopy. *J. Magn. Res.* 53:521–528.

Brunne, R. M., K. D. Berndt, P. Güntert, K. Wüthrich, and W. F. van Gunsteren. 1995. Structure and internal dynamics of the bovine pancreatic trypsin inhibitor in aqueous solution from long-time molecular dynamics simulations. *Proteins Struct. Funct. Genet.* 23:49–62.

Brunne, R. M., E. Liepinsh, G. Otting, K. Wüthrich, and W. F. van Gunsteren. 1993. Hydration of proteins: a comparison of experimental residence times of water molecules solvating the bovine pancreatic trypsin inhibitor with theoretical model calculations. *J. Mol. Biol.* 231: 1040–1048.

Campbell, I. D., C. M. Dobson, and R. J. P. Williams. 1975. Assignment of the ^1H NMR spectra of proteins. *Proc. R. Soc. Lond. Ser. A.* 345: 23–40.

De Jong, E. A. M., C. A. A. Claesen, C. J. M. Daemen, B. J. M. Harmsen, R. N. H. Konings, G. I. Tesser, and C. W. Hilbers. 1988. Mapping of ligand binding site on macromolecules by means of spin-labelled ligand and 2D difference spectroscopy. *J. Magn. Res.* 80:197–213.

Dwek, R. A., J. C. A. Knott, D. Marsh, A. C. McLaughlin, E. M. Press, N. C. Price, and A. I. White. 1975. Structural studies on combining site of myeloma protein MOPC315. *Eur. J. Biochem.* 53:5–59.

Endo, K., I. Morishima, and T. Yonezawa. 1977. Use of a stable free radical as a NMR spin probe for studying intermolecular interactions. XIV. A proton relaxation study of the hydrogen bond involving a stable free radical. *J. Chem. Phys.* 67:4760–4767.

Esposito, G., A. Lesk, H. Molinari, A. Motta, N. Niccolai, and A. Pastore. 1992. Probing protein structure by solvent perturbation of nuclear magnetic resonance spectra. *J. Mol. Biol.* 224:659–670.

Esposito, G., A. Lesk, H. Molinari, A. Motta, N. Niccolai, and A. Pastore. 1993a. Probing protein structure by solvent perturbation of NMR spectra. II. Determination of surface and buried residues in homologous proteins. *Biopolymers.* 33:839–846.

Esposito, G., H. Molinari, A. Motta, and N. Niccolai. 1989. A 2D NMR delineation of the solvent exposure of protein nuclei from paramagnetic relaxation filtering. Proceedings of the 23rd National Convention Gruppo Discussione Risonanze Magnetiche, Cagliari, Italy. 11.

Esposito, G., H. Molinari, M. Pegna, N. Niccolai, and L. Zetta. 1993b. A ^1H NMR study on the interaction of aminoxyl paramagnetic probes with unfolded peptides. *J. Chem. Soc. Perkin Trans.* 2:1531–1534.

Fesik, S. W., G. Gemmecker, E. T. Olejniczak, and M. Petros. 1991. Identification of solvent-exposed regions of enzyme-bound ligands by nuclear magnetic resonance. *J. Am. Chem. Soc.* 113:7080–7081.

Griesinger, C., G. Otting, K. Wüthrich, and R. R. Ernst. 1988. Clean TOCSY for ^1H spin system identification in macromolecules. *J. Am. Chem. Soc.* 110:7870–7872.

Improta, S., H. Molinari, A. Pastore, R. Consonni, and L. Zetta. 1995a. Probing protein structure by solvent perturbation of NMR spectra. A comparison with photochemically induced dynamic nuclear polarization techniques applied to native α-lactalbumin. *Eur. J. Biochem.* 227: 78–86.

Improta, S., H. Molinari, A. Pastore, R. Consonni, and L. Zetta. 1995b. Probing protein structure by solvent perturbation of NMR spectra. Photochemically induced dynamic nuclear polarization and paramagnetic perturbation techniques applied to the study of the molten globule state of α-lactalbumin. *Eur. J. Biochem.* 227:87–96.

Lee, B., and F. M. Richards. 1971. The interpretation of protein structures: estimation of static accessibility. *J. Mol. Biol.* 55:379–400.

Lichtarge, O., O. Jardetzky, and C. H. Li. 1987. Secondary structure determination of human β-endorphin by ^1H NMR spectroscopy. *Biochemistry.* 26:5916–5925.

Kosen, P. A., R. M. Scheek, H. Naderi, V. J. Basus, S. Manogaran, P. G. Schmidt, N. J. Oppenheimer, and I. D. Kuntz. 1986. Two dimensional ^1H NMR of three spin-labelled derivatives of BPTI. *Biochemistry.* 25:2356–2364.

Molinari, H., G. Esposito, R. Consonni, M. Pegna, and L. Zetta. 1992. Distance evaluation via heteronuclear SQC-NOESY experiments. *J. Biomol. NMR.* 2:289–299.

Moonen, C. T. W., R. M. Scheek, R. Boelens, and F. Muller. 1984. The use of 2D NMR spectroscopy and 2D difference spectra in the elucidation of the active center of *Megasphoena elsdenii* flavodoxin. *Eur. J. Biochem.* 141:323–330.

Morris, G. A., and R. Freeman. 1978. Selective excitation in Fourier transform nuclear magnetic resonance. *J. Magn. Res.* 29:433–462.

Niccolai, N., A. Bonci, M. Rustici, M. Scarselli, P. Neri, G. Esposito, P. Mascagni, A. Motta, and H. Molinari. 1991. NMR delineation of inner and outer protons from paramagnetic relaxation perturbations in 1D and 2D spectra of peptides. *J. Chem. Soc. Perkin Trans.* 2:1453–1457.

Nirmala, N. R., and G. Wagner. 1988. Measurement of ^{13}C relaxation times in proteins by two-dimensional heteronuclear ^1H-^{13}C correlation spectroscopy. *J. Am. Chem. Soc.* 110:7557–7558.

Petros, A. M., L. Mueller, and K. D. Kopple. 1990. NMR identification of protein surface using paramagnetic probes. *Biochemistry.* 29: 10041–10048.

Petros, A. M., P. Neri, and S. W. Fesik. 1992. Identification of solvent-exposed regions of an FK-506 analog, ascomycin, bound to FKBP using a paramagnetic probe. *J. Biomol. NMR.* 2:11–18.

Piotto, M., V. Saudek, and V. Sklenar. 1992. Gradient-tailored excitation for single-quantum NMR spectroscopy of aqueous solutions. *J. Biomol. NMR.* 2:661–666.

Qiu, Z. W., D. M. Grant, and R. J. Pugmire. 1982. Paramagnetic carbon-13 shifts induced by the free radical 2,2,6,6-tetramethylpiperidinyl-1-oxy. 1. Simple aromatic and paraffinic hydrocarbons. *J. Am. Chem. Soc.* 104:2747–2753.

Qiu, Z. W., D. M. Grant, and R. J. Pugmire. 1984. Paramagnetic carbon-13 shifts induced by the free radical TEMPO. 2. Nitrogen heterocycles. *J. Am. Chem. Soc.* 106:557–560.

Richarz, R., H. Nagayama, and K. Wüthrich. 1980. Carbon-13 nuclear magnetic resonance relaxation studies of internal mobility of the polypeptide chain in basic pacreatic trypsin inhibitor and a selectively reduced analogue. *Biochemistry.* 19:5189–5194.

Scarselli, M., G. Esposito, H. Molinari, M. Pegna, L. Zetta, and N. Niccolai. 1995. The use of paramagnetic probes for NMR investigations of biomolecular structures and interactions. *In* From Neural Networks and Biomolecular Engineering to Bioelectronics. C. Niccolini, editor. Plenum Press, New York. 95–102.

Schmidt, P. G., and I. D. Kuntz. 1984. Distance measurements in spin labeled lysozyme. *Biochemistry.* 23:4261–4266.

Solomon, I., and N. Bloembergen. 1956. Nuclear magnetic interactions in the HF molecule. *J. Chem. Phys.* 25:261–273.

Wagner, G., W. Braun, T. F. Havel, T. Schaumann, N. Go, and K. Wüthrich. 1987. Protein structures in solution by nuclear magnetic resonance and distance geometry. The polypeptide fold of the BPTI determined using two different algorithms, DISGEO and DISMAN. *J. Mol. Biol.* 196:611–639.

Wagner, G., I. Stassinopoulou, and K. Wüthrich. 1984. Amide-proton exchange studies by two-dimensional correlated ^1H NMR in two chemically modified analogs of the basic pancreatic trypsin inhibitor. *Eur. J. Biochem.* 145:431–436.

Wien, R. W., J. D. Morrisett, and H. M. McConnell. 1972. Spin label induced nuclear relaxation. Distances between bond saccharides, histi-

dine-15 and tryptophan-123 on lysozyme in solution. *Biochemistry.* 11:3707–3716.

Williams, R. J. P. 1989. NMR studies of mobility within protein structure. *Eur. J. Biochem.* 183:479–497.

Wlodawer, A., J. Nachman, G. L. Gilliland, W. Gallagher, and C. Woodward. 1987. Structure of form III crystals of bovine pancreatic trypsin inhibitor. *J. Mol. Biol.* 198:469–480.

Zetta, L., R. Consonni, A. De Marco, R. Longhi, E. Manera, and G. Vecchio. 1990. Opioid peptides in micellar systems: conformational analysis by CD and by one-dimensional and two-dimensional ^{1}H-NMR spectroscopy. *Biopolymers.* 30:899–909.

Zetta, L., and R. Kaptein. 1984. Interaction of β-endorphin with sodium dodecyl sulfate in aqueous solution. ^{1}H-NMR investigation. *Eur. J. Biochem.* 145:181–186.